NANOSYSTEMS:
PHYSICS, CHEMISTRY, MATHEMATICS

Bukharov D.N., et al. *Nanosystems: Phys. Chem. Math.*, 2025, **16** (4), 427–436.
http://nanojournal.ifmo.ru
DOI 10.17586/2220-8054-2025-16-4-427-436

Original article

Modeling of graphitization in CVD diamond under the action of laser radiation

Dmitry N. Bukharov[1,a], Timur A. Khudaiberganov[1,b], Alexey O. Kucherik[1,c], Sergey M. Arakelian[1,d]

[1]A. G. and N. G. Stoletov Vladimir State University, 87 Gorykogo st, 600000, Vladimir, Russia

[a]buharovdn@gmail.com, [b]thomasheisenberg@mail.ru, [c]kucherik@vlsu.ru, [d]arak@vlsu.ru

Corresponding author: D. N. Bukharov, buharovdn@gmail.com

PACS 02.60.Cb

ABSTRACT A model describing the graphitization of CVD diamond under the action of femtosecond laser radiation is proposed. The model combines thermal and kinetic aspects, taking into account the phase transition of diamond into graphite upon reaching critical conditions (temperature or charge carrier density). A mathematical model of the temperature field for a laser source is presented taking into account the dependencies for enthalpy and polarization. A mathematical model of the diamond-graphite phase transition under laser radiation is developed within the framework of the charge carrier density equation. The governing equations were presented in finite-difference form and discretized using a five-point stencil on a uniform grid. The finite-difference equations were solved using the explicit Euler scheme. Numerical simulation of diamond graphitization allowed us to estimate the key features of the initial stage of the process.

KEYWORDS modeling, graphitization, thermodynamic model of graphitization, numerical methods, phase transition.

ACKNOWLEDGEMENTS The research was carried out within the framework of the scientific project FZUN-2024-0018.

FOR CITATION Bukharov D.N., Khudaiberganov T.A., Kucherik A.O., Arakelian S.M. Modeling of graphitization in CVD diamond under the action of laser radiation. *Nanosystems: Phys. Chem. Math.*, 2025, **16** (4), 427–436.

1. Introduction

Currently, materials based on artificial diamonds and their modifications can confidently be considered promising for the implementation of the innovative element base of modern micro-nanoelectronics [1, 2] and nanophotonics [3, 4] devices, for example, detectors, quantum sensors [5–7], as well as components of small-sized lasers [8]. An important aspect in the development and construction of such devices is the possibility of forming controlled electrically conductive structures in a sample of synthetic diamond [9, 10].

One of the effective and universal methods that makes possible modification of the diamond structure in a given direction and synthesis of sufficiently high-quality electrically conductive graphitized structures with a developed surface is controlled local laser modification of the sample structure by inducing different configurations of inhomogeneities in it [11, 12]. We implemented this local laser modification (the scheme is presented in section 2) and synthesized the filamentous graphitized structures.

The analysis of the optical images of the samples we obtained showed that the laser-induced method of synthesizing graphitized regions is controllable and allows us to form the required topological and structural characteristics of the samples. These properties are influenced by a number of parameters of the experimental laser synthesis scheme: the energy of the laser pulse and its duration, and others. The process of assessing the role and influence of these parameters on the implemented configuration states of samples can be optimized by using the capabilities of mathematical/computer modeling.

To date, there are a number of models describing the process of laser graphitization [13–19]. In particular, works [13, 14] considered the model of temperature fields during laser processing of diamond crystals, taking into account their graphitization, which was caused by the anisotropy of the thermophysical properties of graphite. In [15], a finite element model using powder absorption theory was developed and implemented in the Ansys environment describing a temporary change in diamond temperature during graphitization. In [16, 17], using molecular dynamic (MD) modeling, graphitization of the CVD diamond surface was studied. In our previous works [18, 19], the fractal models of the first approximation have been proposed to describe the growth of laser-induced graphitized structures formed taking into account diamond microcracks. These models are implemented in the diffusion approximation within the framework of a cellular automaton with a Neumann neighborhood. Thus, the models developed earlier are, to a certain extent, imitative in nature and contain indirect connections of their parameters with real physical quantities involved in real synthesis, and also do not take into account the entire set of physical processes occurring during laser graphitization. This article

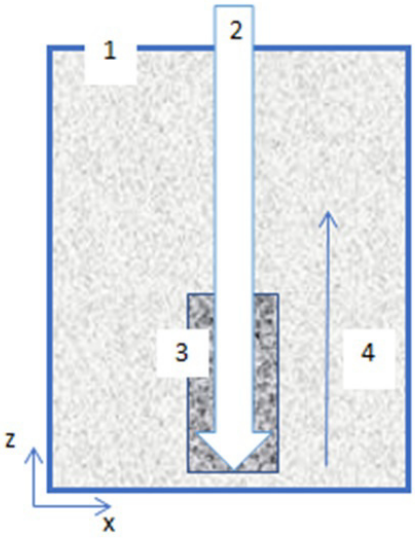

FIG. 1. The scheme of laser synthesis of graphitized filamentous regions: 1 - CVD diamond with defects, 2 - laser radiation, 3 - graphitized area, 4 - the direction of growth of the graphitization area

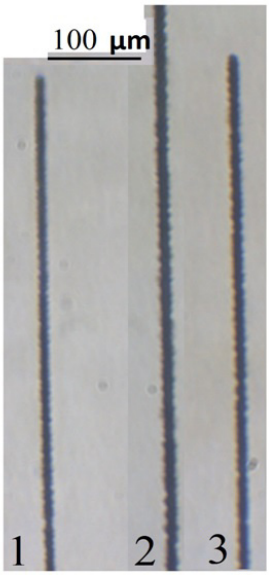

FIG. 2. Optical images of graphitized filamentous structures at $E = 0.184$ mJ, $u = 12.5$ μm, $Df = 1.22$ (1), $E = 0,288$ mJ, $u = 14.2$ μm, $D_f = 1.24$ (2), $E = 0,43$ mJ, $u = 15.4$ μm, $D_f = 1.25$ (3)

proposes an extended model of laser graphitization based on in-depth description of the thermodynamic processes of laser graphitization, taking into account the diamond-graphite phase transition when a critical temperature and charge carrier density are reached, which explicitly contains a large number of physical parameters related to the actual synthesis scheme.

2. Description of the synthesis scheme of graphitized structures in CVD diamond and the physical processes of their laser synthesis for modeling the structure of the modified region

According to the scheme shown in Fig. 1, we obtained various filamentous graphitized regions in CVD diamond. The CVD diamond sample provided by Almaznaya Dolina Group was exposed to a femtosecond Yb:KGW laser system (Avesta, Russia) at a wavelength of λ = 1030 nm, pulse duration τ = 500 fs, with an operating pulse repetition frequency of 10 kHz with varying pulse energy E. A beam of a Gaussian profile with a radius of 5 microns was focused on the near-surface layer of the lower face at a depth of 250 microns. The increase in energy in the pulse was accompanied by a slight increase in the diameter of the obtained samples (u) (about 12–23 %), as well as an increase in the fractal dimension (D_f) estimated by the boxcounting method [20].

A study of the dynamics of the process of laser modification of artificial diamond CVD diamond during the synthesis of a graphitized region in it demonstrates that the defining process is the occurrence of microcracks with numerous "activation centers" that initiate the propagation of a thermally stimulated graphitization wave into the surrounding diamond volume [21]. Thus, it can be argued that the wave propagation process causing graphitization of regions in CVD diamond is thermodynamic in nature.

During the laser exposure, a sufficiently powerful short laser pulse hit the diamond at a wavelength of 1030 nm. Although an ideal diamond is transparent for this wavelength, energy was absorbed at defects (nitrogen vacancies) or in high-intensity regions where diamond atoms were forced to absorb five photons at once. This process knocked out electrons, creating high-energy free electrons. The electric field of the laser accelerated these electrons, causing avalanche ionization: electrons collided with atoms, knocking out more and more electrons (this process was described by the equation of dynamics of the concentration of charged carriers), and the concentration of high-energy electrons increased exponentially. When the electron concentration (N) or temperature (T) reached a critical value, the strong sp3 bonds of diamond were destroyed, turning it into graphite. Thus, as soon as the first section of graphite appeared, it began to actively absorb laser radiation, accelerating heating and ionization around it, thereby initiating graphitization of areas next to it.

Thus, from the point of view of thermodynamics, the laser graphitization process can be considered as a three-stage process. At the first stage, the diamond is heated to the temperature of the phase transition T_c. At the second stage, a phase transition is implemented at a constant temperature $T = T_c$. At the third stage, graphite is heated after the phase transition is completed.

Graphitization occurs when the carrier density in a cell reaches a critical value sufficient for the diamond → graphite phase transition. This is due to the fact that high concentration of hot electrons breaks the sp3 bonds of diamond, converting them into sp2 bonds of graphite. The carrier density increases due to carrier generation from two-photon absorption in diamond due to defects and is further enhanced by avalanche ionization under the action of a laser field. When the carrier density exceeds the critical value of N_c, the electron energy becomes sufficient to overcome the activation barrier of the phase transition (analogous to the temperature of the T_{cr} in the thermal model) [21]. Then you can set the matrix of phase composition as $M = \left[M_{ijl}^m\right] = \begin{cases} 0,\ diamond \\ 1,\ graphite \end{cases}$. It obeys the condition $M_{ijl}^{m+1} = \begin{cases} 0,\ N_{ijl}^m < N_c \\ 1,\ N_{ijl}^m \geq N_c \end{cases}$, where i, j, l correspond to the numbers of spatial cells, and m corresponds to the discrete time t.

Thus, to model the structure of a graphitized region, it is necessary to describe the dynamics of thermal processes (temperature field), as well as processes of changes in carrier density, the achievement of critical values of which leads to a change of the phase composition. Fig. 3 shows a diagram of the processes taken into account when modeling the graphitization process.

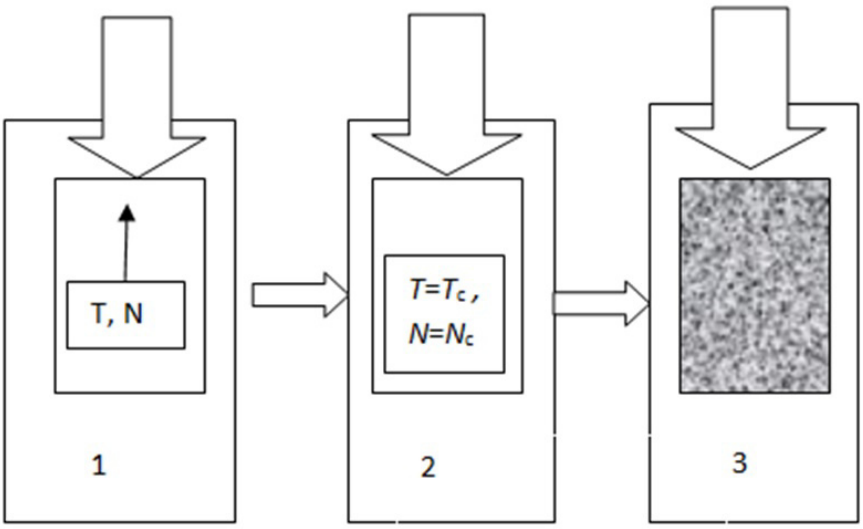

FIG. 3. The physical processes taken into account in the graphitization model are: 1 – diamond heating: an increase in the temperature of the heated area (T), accompanied by an increase in carrier density (N), 2 – reaching a critical temperature (T_c), reaching a critical carrier density (N_c)

3. Laser graphitization mathematical model description

The model of the temperature field during laser graphitization was represented by the thermal conductivity equations for the diamond and graphite phases (equations 1,2), supplemented by initial and boundary conditions (ratio 6). The equations of thermal conductivity are formulated in the stationary case, as well as taking into account assumptions for thermally insulated boundaries (ratio 6), and also do not take into account heat transfer at the boundaries from graphite and diamond sections.

The thermal conductivity equation for the diamond phase had the form [15]:

$$\rho_d c_d \frac{\delta T}{\delta t} = \nabla \left(k_d \nabla T\right) + Q_l \tag{1}$$

where $Q_l = \alpha_d(I) \cdot I(x, y, z, t)$ [15] is a heat source defined by the spatial distribution of the laser pulse, $\alpha_d(I) = \alpha_5 I^4 + \alpha_2^{def} I$ is the nonlinear absorption coefficient and $\alpha_5 \sim \sigma_5$ is the diamond five-photon absorption coefficient, σ_5 is the five photon absorption cross section and $\alpha_2^{def} \sim \sigma_5 \rho_{def}$ is the two-photon absorption at the color centers [23], where ρ_{def} is the defect density, $k_d(x, y, z)$ is the thermal conductivity coefficient, c_d is the diamond heat capacity, ρ_d is the diamond density.

Thus, equation (1) is the thermal conductivity equation for diamond, where the heat source is determined by two- and five-photon absorption, with thermal conductivity and absorption coefficients taken from [23], taking into account the high thermal conductivity of diamond (∼2000 W/m·K).

The laser beam intensity (I) at depth z, in cylindrical coordinates, varied according to the following equations [23]:

$$I = f(t) \begin{cases} (1-R)\, I \dfrac{\left[F\left(r,z\right)\left(1-\beta_2\left(1-R\right)z\right) - \beta_2\left(1-R\right)I\right]}{\left(1+\beta_2\left(1-R\right)I \cdot z\right)^2},\ diamond \\ F\left(r,z\right) e^{-\alpha_g z} - \alpha_g I,\ graphite \end{cases} \tag{2}$$

where $f(t)$ describes pulsed laser radiation, $F(r,z)$ makes it possible to take into account the geometric divergence of the beam, β_2 is the two-photon absorption coefficient at the diamond color centers, R is the reflection coefficient, and α_g is the graphite absorption coefficient. The function that takes into account the geometric divergence of the beam looks like $F(r,z) = I_s \frac{\xi\left(-2\left(1+\xi^2\right)+4r^2/w_0^2\right)}{\left(1+\xi^2\right)^2}$, where is the normalized by the Rayleigh length distance to the focal plane (the focus was determined if $\xi = 0$), z_f is the depth of focus, $z_R = \frac{\pi w_0^2}{\lambda}$ is the Rayleigh length, $r = \sqrt{x^2+y^2}$ is the radial distance, $I_s = I_0 \left(\frac{w_0}{w(z)}\right) \exp\left(-\frac{2r^2}{w(z)^2}\right)$ is the Gaussian beam intensity, $w(z) = w_0\sqrt{1+\xi^2}$ is the beam radius.

Pulsed laser radiation is described using the modulation of the radiation intensity by the function [24]:

$$f(t) = \exp\left(-\frac{\left(t_{rel}-\tau/2\right)^2}{2\left(\tau/2.35\right)^2}\right)\left(\Theta\left(t_{rel}\right)-\Theta\left(t_{rel}-\tau\right)\right), \tag{3}$$

where Θ is the Heaviside function.

The first multiplier sets the Gaussian pulse profile with the pulse duration τ and the Gaussian profile width $\tau/3$, where $t_{rel} = t - \lfloor t/\Delta t \rfloor$ is the the time relative to the start of the current pulse. Δt is the time interval between pulses, $\lfloor t/\Delta t \rfloor$ is the integer part function that returns the index of the current pulse, determining which pulse time t belongs to. The second multiplier is the window that limits the t_{rel} time to the half interval $[t_{rel}-\tau, t_{rel})$.

Thus, equation (2) takes into account the Gaussian beam profile, geometric divergence, and absorption, which is physically justified by the need to describe the local energy distribution in the material.

The thermal conductivity equation for the graphite phase has the form [15]:

$$\rho_g c_g \frac{\delta T}{\delta t} = \nabla\left(k_g \nabla T\right) + Q_l', \tag{4}$$

where $Q_l' = \alpha_g(I)\cdot I(x,y,z,t)$ [15] is the heat source, α_g is the graphite absorption coefficient, exponentially dependent on temperature, k_g is the graphite thermal conductivity coefficient c_g is the graphite heat capacity, ρ_g is the graphite density.

Equation (4) extends the thermal conductivity model to graphite. The diamond-graphite phase transition critical temperature T_c is determined from the condition: $\Delta G(T_c) = 1273 + 4.64T$ [25], where $G = H - TS + G_d$ [25] is the Gibbs energy, G_d is the defects Gibbs energy, at the same time $\Delta G_d = \gamma\rho_d$ [26], γ is the defects energy, ρ_d is the defects density, H is the enthalpy, S is the entropy. Thus, we can assume that $T_c = 2000$ K [27].

Equations 1-4 are supplemented with the initial conditions:

$$T(x,y,z,0) = T_0. \tag{5}$$

Conditions of the second kind are set at the lateral and lower boundaries of the design area, taking into account that they are thermally insulated:

$$\frac{\delta T}{\delta n}(\partial\Omega) = 0, \tag{6}$$

where $\partial\Omega$ is the boundary of the region, and n is the normal to the boundary.

The enthalpy (H) equation allowes us to naturally take into account the latent heat of the phase transition and has the form [28]:

$$\frac{\delta H}{\delta t} = \kappa\nabla^2 H + Q, \tag{7}$$

where κ is the thermal conductivity.

Temperature is related to enthalpy by the relation [29]:

$$T = \begin{cases} \dfrac{H}{\rho_d c_d}, & \dfrac{H}{\rho_d c_d} < T_c \\ T_{cr}, & H < \rho_d c_d T + \rho_d \Phi \\ T_{cr} + \dfrac{H - \left(\rho_d c_d T_{cr} + \rho_d \Phi\right)}{\rho_g c_g}, & \text{graphite} \end{cases} \tag{8}$$

where Φ is the latent heat of the phase transition.

The enthalpy is a function of energy which allowes us to simulate a phase transition without an obvious discontinuity in temperature T.

Equation (8) includes the latent heat of the diamond-graphite phase transition, determining the energy barrier for breaking sp3 bonds and forming sp2 bonds. The diamond-graphite transition is modeled using critical parameters (T_c, N_c), which is associated with the breaking of sp3 bonds and the formation of sp2 bonds at high temperatures and carrier densities.

The heat source is determined by the intensity of the laser radiation in the volume of the material and the absorption coefficient: $Q = \begin{cases} \beta_2 I^2, \text{ diamond} \\ \alpha_g I, \text{ graphite} \end{cases}$, where β_2 is the two-photon coefficient.

To describe the generation and dynamics of hot electrons, Fick's equation for the number of charge carriers N is used, which took into account their diffusion, laser generation, and recombination, but without taking into account the polarization. The exclusion of the polarization dynamics equation from the system of equations is justified by the use of a quasi-static (adiabatic) approximation. The physical basis of this approach lies in a significant difference in time scales: the time to establish electronic polarization in diamond is orders of magnitude shorter than both the duration of the laser pulses we use and the characteristic carrier recombination time.

This allows us to assume that the response of the medium to the laser field is inertia-free.

The equation for the carrier density has the form [30]:

$$\frac{\delta N}{\delta t} - D_N(M)\nabla^2 N = G(M) - \gamma_n(M)N, \tag{9}$$

where D_N is the carrier diffusion coefficient, which differs for diamond and graphite, G is the phase-dependent carrier generation rate, γ_n is the carrier recombination rate, respectively.

Equation (9) describes the dynamics of the charge carrier density taking into account carrier generation by two-photon absorption and avalanche ionization, as well as the recombination with a typical time of $\sim 10^{-12}$ s. It is supplemented by a boundary condition:

$$N\left(\partial\Omega\right) = 0. \tag{10}$$

The model's equations are related through the laser intensity, which controls thermal processes and carrier generation, with physical parameters (absorption coefficients, heat capacity, diffusion).

The model has the following assumptions and simplifications:

1. Five-photon absorption contributes only at high laser intensities;

2. In equation (7), the latent heat of the diamond-graphite phase transition is approximated by a piecewise linear function, which is justified by the need to ensure energy continuity during the transition of sp3→sp2 bonds and simplify numerical calculations while maintaining physical accuracy;

3. Equations (1) and (4) assume homogeneous thermal and optical properties of diamond and graphite (thermal conductivity ∼2000 W/m·K for diamond, ∼100 W/m·K for graphite), which can be justified by the fact that local inhomogeneities in CVD diamond are minimal at the considered laser focus scales.

Thus, the equations, initial and boundary conditions (1)–(10) formed a mathematical model of laser graphitization.

4. Description of the numerical model of laser graphitization

The model equations are considered on a three-dimensional computational domain. The computational domain on which the equations of the mathematical model of the temperature field were discretized represented a rectangular parallelepiped with sides of lengths L_x, L_y, L_z, respectively. A uniform spatial grid consisting of $N_x = N_y = N_z$ cells, which were cubes with a side $\Delta = \frac{L_x}{N_x}$, is superimposed on the calculated area. Thus, the value Δ determines the spatial integration step. The laser beam is focused into a central cell with coordinates (i_c, j_c, k_c). The time integration step is constant Δ_t taking into account that all properties and parameters of the system remains constant during this time interval. Then the time t elapsed over m iterations is defined as $t_m = \Delta_t m$.

The equation describing the temperature field is represented in matrix form as $T = \left[T_{ijl}^m\right]$. It is reduced to a recurrent matrix equation $T^m = \left[T_{ijl}^m\right]$, where i, j, l were spatial indexes ($i = 1, ...N_x$, $j = 1, ...N_y$, $l = 1, ...N_z$), and m is the iteration number, which has the form:

$$T^{m+1} = T^m + \frac{\Delta_t}{\rho c_p}\left(kLT^m + Q^m\right), \tag{11}$$

where $T^m = \left[T_{ijl}^m\right]$ is the temperature matrix after m iterations, Δ_t is the time step, ρ is the density, c_p is the specific heat, k is the thermal conductivity, L is the discrete Laplace operator, $Q^m = \left[Q_{ijl}^m\right]$ is the matrix of the heat source.

The discrete Laplace operator based on a five-point pattern is implemented [31]:

$$\left(LT^m\right)_{ijl} = \frac{T_{i+1,j,l}^m - 2T_{i,j,l}^m + T_{i-1,j,l}^m}{\Delta^2} + \frac{T_{i,j+1,l}^m - 2T_{i,j,l}^m + T_{i,j-1,l}^m}{\Delta^2} + \frac{T_{i,j,l+1}^m - 2T_{i,j,l}^m + T_{i,j,l-1}^m}{\Delta^2}. \tag{12}$$

The enthalpy matrix $H^m = \left[H_{ijl}^m\right]$ after m iterations is calculated based on the equation:

$$H^{m+1} = H^m + \Delta_t\left(kLT^m + Q^m\right). \tag{13}$$

For the discrete case, the carrier concentration is set by a matrix with matrix elements corresponding to the carrier density $N^m = \left[N^m_{ijl}\right]$ determined on the basis of the equation

$$\frac{N^{m+1}_{i,j,l} - N^m_{i,j,l}}{\Delta_t} - D_N(M^m_{i,j,l})LN^m_{i,j,l} = G^m_{i,j,l}(M^m_{i,j,l}) - \gamma_n(M^m_{i,j,l})N^m_{i,j,l}, \quad (14)$$

$$(LN^m)_{ijl} = \frac{N^m_{i+1,j,l} - 2N^m_{i,j,l} + N^m_{i-1,j,l}}{\Delta^2} + \frac{N^m_{i,j+1,l} - 2N^m_{i,j,l} + N^m_{i,j-1,l}}{\Delta^2} + \frac{N^m_{i,j,l+1} - 2N^m_{i,j,l} + N^m_{i,j,l-1}}{\Delta^2}. \quad (15)$$

The rate of the carrier generation has the form: $G = \begin{cases} \dfrac{\beta_2 I^2 N}{2\hbar\omega}, \text{ diamond} \\ N\mu_n E_c, \text{ graphite} \end{cases}$, where N is the concentration of defects (nitrogen vacancies); $E_c = \sqrt{I(x,y,z,t)}\exp(i\omega t)$ is the field in the diamond, $\hbar$ is the reduced Plank constant, μ_n is the mobility of electrons, ω is the frequency of laser radiation.

5. Laser graphitization modeling results

The numerical model is implemented in Python using the JAX library for efficient GPU calculations [32]. 64-bit precision is used for all calculations. Vectorized operations using vmmap and automatic compilation (jit) of critical code sections are used to speed up calculations [32]. The Euler method of the first order is used to solve differential equations [33].

The main physical parameters of the model describing the diamond-graphite system has the following values: the diffusion coefficient of charge carriers $D_N = \begin{cases} 5\times10^{-3}, \text{ diamond} \\ 1\times10^{-4}, \text{ graphite} \end{cases}$ (m^2/s) [34, 35], the rate of recombination of charge carriers $\gamma_n = \begin{cases} 1\times10^{9}, \text{ diamond} \\ 1\times10^{11}, \text{ graphite} \end{cases}$ (s^{-1}) [34, 36], the coefficient of thermal conductivity $k = \begin{cases} 2000, \text{ diamond} \\ 100, \text{ graphite} \end{cases}$ W/(m·K) [37,38], the density $\rho = \begin{cases} 3510, \text{ diamond} \\ 2250, \text{ graphite} \end{cases}$ (kg/m^3) [37,38], the specific heat capacity $c_p = \begin{cases} 509, \text{ diamond} \\ 710, \text{ graphite} \end{cases}$ J/(kg·K) [36, 39], the specific heat of the phase transition Φ=1.2×10^5 J/kg [40], the two-photon absorption coefficient a_2=4×10^{-11} m/W [41], the linear absorption coefficient in graphite a_g=1×10^5 m^{-1} [42], the group refractive index $n_g = \begin{cases} 2.4, \text{ diamond} \\ 2.6, \text{ graphite} \end{cases}$ [43,44].

The simulation was performed for a laser system operating in pulsed mode at a wavelength of $\lambda = 1030 \cdot 10^{-9}$ m, generating 100 pulses with an intensity of $I = 10^{12}$ W/m^2, a pulse duration of 500·10^{-15}s, an interval between pulses $\Delta t = 10^{-12}$ s and a beam radius of $w_0 = 5$ microns, which focused on depth $d = 250$ microns. The reflection coefficient at the boundary (R) was assumed to be 0.2 The lengths of the sides of the calculated area were assumed to be L_x= 500 microns, $L_y = L_z = 200$ microns, the number of nodes of the spatial grid was assumed to be $N_x = N_y = 60$, $N_z = 120$. The simulation time was 0.1 s, which corresponded to the time of real graphitization [18]. The simulation time step was 10^{-12} s, the value of which guaranteed the stability of the applied explicit difference scheme for solving model equations. The threshold temperature of the diamond-graphite phase transition was assumed to be $T_c = 2000.0$ K. The threshold carrier density for graphitization was estimated as $N_c = 10^{24}$ m^3. The initial temperature of the system was assumed to be $T_0 = 300$ K. The initial fraction of graphite was estimated to be 1 %. At the initialization stage of the model, the distribution of the initial graphite clusters, which initiated the graphitization process, was placed in the computational domain.

Figure 4 shows typical simulation results of the above parameters in the form of two-dimensional sections of the computational domain.

Numerical modeling of diamond graphitization in the range of 0.1 microseconds revealed the key features of the initial stage of the process. Initially, a system of defects was located in the design area, pressed down by graphite filaments with a radius of 0.2 microns, oriented from the surface to the focal plane (Fig. 4a). Laser radiation initiated the growth of charge carriers in the graphite phase, and when the N_c threshold is exceeded (Fig. 1b), the graphite phase begins to expand on the surface of the filaments due to the avalanche ionization mechanism. After pulsed laser exposure (Fig. 4b) graphite filaments merge, and the graphite phase exhibits growth unrelated to the temperature gradient, spreading transversely perpendicular to the direction of the laser radiation (Fig. 4d).

The fractal dimension was estimated for the model sample from Fig. 4b. The boxcounting method was used for evaluation [20]. The value of the fractal dimension was 1.26.

Figure 5 shows a simulation of the graphite fraction over time for different parameters of the laser system for 100 pulses and varying the maximum laser intensity ($I_{\max}$), as well as the beam radius (w).

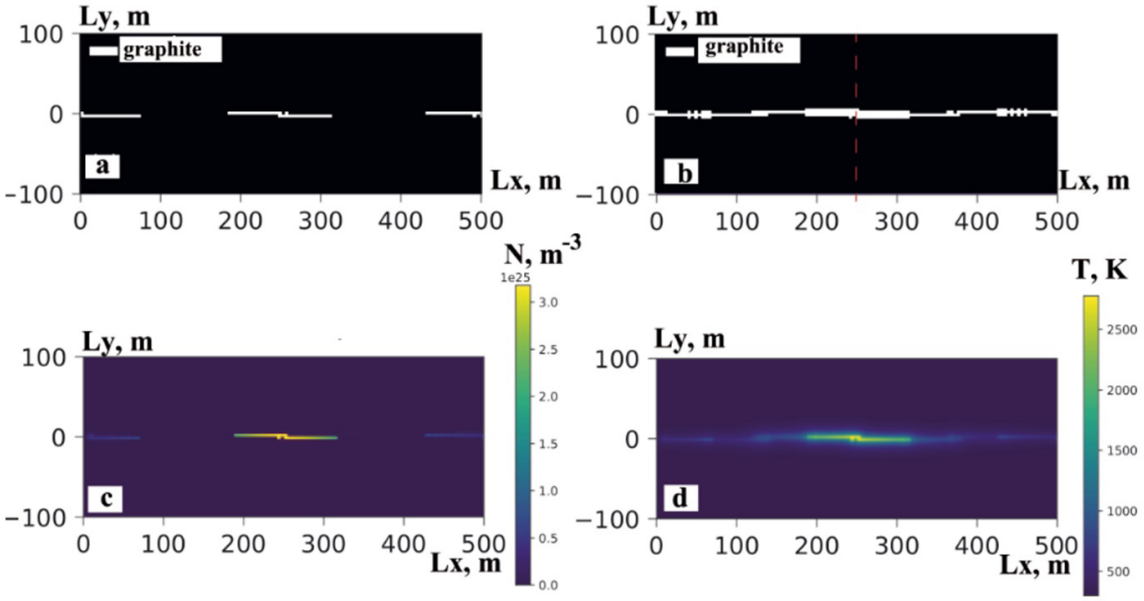

FIG. 4. Graphitization modeling results: of the graphite phase initial distribution (a); distribution of the graphite phase after exposure to pulsed laser radiation (b); distribution of charge carriers after exposure to pulsed laser radiation (c); temperature map after exposure to pulsed laser radiation (d)

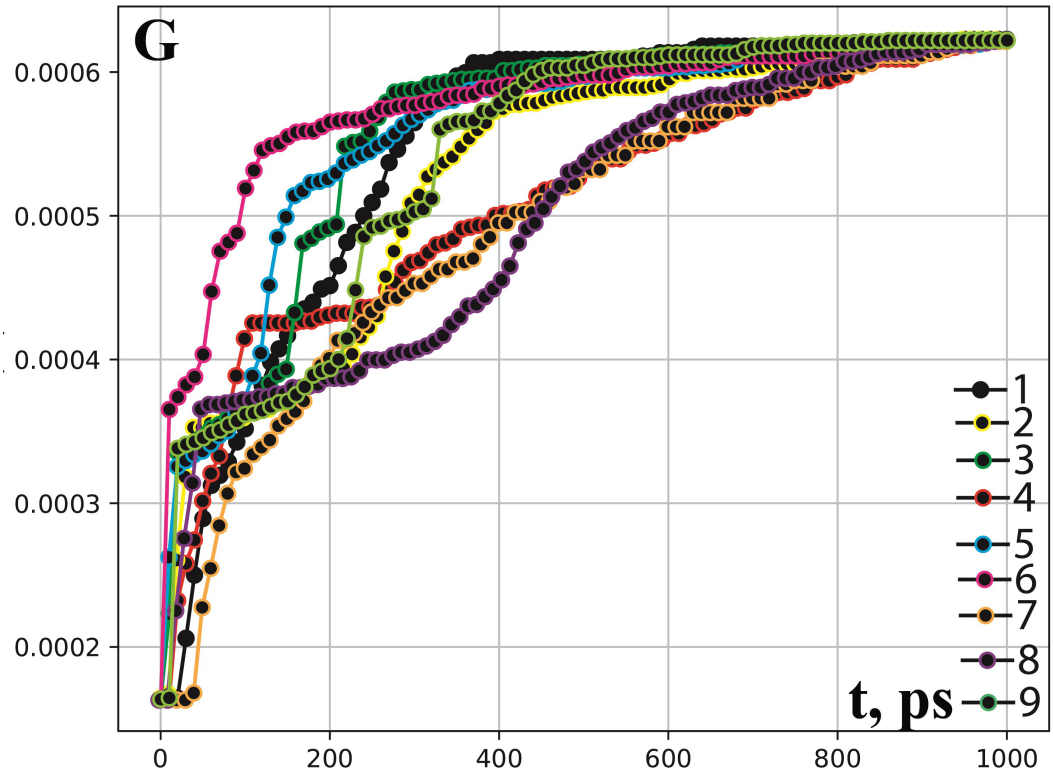

FIG. 5. The modeled dependence of the graphite fraction on time: $I_{\max} = 10^{12}$ W/m^2, $w = 2$ μm (1), $I_{\max} = 10^{12}$ W/m^2, $w = 5$ μm (2), $I_{\max} = 10^{12}$ W/m^2, $w = 10$ μm (3), $I_{\max} = 0.5 \cdot 10^{12}$ W/m^2, $w = 2$ μm (4), $I_{\max} = 0.5 \cdot 10^{12}$ W/m^2, $w = 5$ μm (5), $I_{\max} = 0.5 \cdot 10^{12}$ W/m^2, $w = 10$ μm (6), $I_{\max} = 2 \cdot 10^{12}$ W/m^2, $w = 2$ μm (7), $I_{\max} = 2 \cdot 10^{12}$ W/m^2, $w = 5$ μm (8), $I_{\max} = 2 \cdot 10^{12}$ W/m^2, $w = 10$ μm (9)

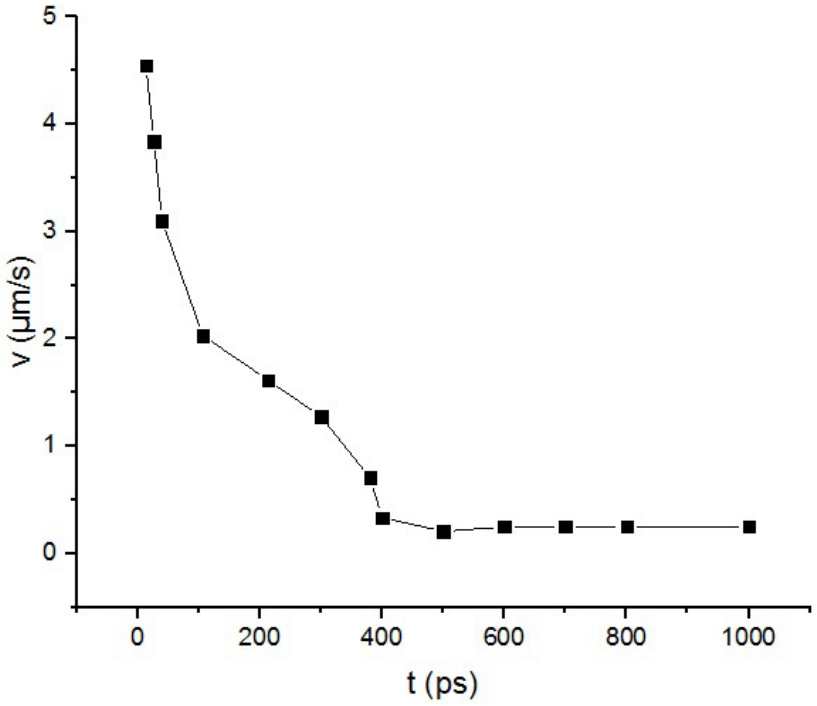

FIG. 6. The modeled average graphitization rate for calculation from Fig. 4

The simulation showed that before reaching the T_c temperature, the growth rate of the graphite phase is proportional to time (t). This fact indicates the predominance of avalanche ionization, when graphite grows in length and width, the rate of the graphite phase slows down significantly (see Fig. 5, Graphs 1-6). At $T > T_c$, the growth of the graphite phase accelerates, following a new dynamic $\sim \sqrt{t}$ (see Fig. 5, Graphs 7, 8 and 9).

After a time interval of about 700 ps, the graphite fraction is saturated and all dependencies are stabilized. This behavior corresponds to the steady-state mode for graphitization rate. Fig. 6 shows an average model estimate of the graphitization rate for calculation from Fig. 4.

To assess the adequacy of the proposed model approximation, the relative modeling error was estimated as the difference between the fractal dimensions for the model sample (Fig. 4) and the average fractal dimension of the samples obtained as a result of laser synthesis (Fig. 2). The value obtained did not exceed 2.34 %, which indicated that the proposed approximation was well adequate. In addition, the modeled dependences on the growth of graphitized structures and the graphitization rate at a qualitative level correspond to similar dependences obtained by us using other laser schemes [18,19,45] as well as by other scientific groups [11,46,47], whose results are presented in the scientific literature.

6. Conclusion

Numerical modeling of diamond graphitization using the proposed model makes it possible to evaluate the key features of the initial stage of the CVD diamond micromodification process.

The presented model takes into account the physical processes that determine laser graphitization, such as laser heating, accompanied by a change in the density of high-energy free electrons, leading to the diamond-graphite phase transition. The model takes into account the real physical parameters of the laser synthesis scheme of graphitized structures, as well as the properties of real samples, such as fractal dimension, which form a connection with the real scheme of micromodification of CVD diamond. The considered model approximation is adequate for describing the process of laser graphitization of diamond, as evidenced by the relative error of the model, which does not exceed 10%. The proposed model allows the evaluation of its results with the results of real laser synthesis by estimating the values of fractal dimensions. The similarity of the fractal dimensions of the model and the sample will allow us to hope for a similar similarity of functional, topology-related properties (optical, electrophysical [48, 49]) of real samples and the models proposed for them. In this regard, such a model approximation has the prospect of being used as a tool for predicting the features of the images of graphitized areas of CVD diamond before their actual synthesis, which will reduce the time and financial costs of experimental studies of the micromodification process of artificial diamonds.

References

[1] Araujo D., Suzuki M., Lloret F., et al. Diamond for Electronics: Materials, Processing and Devices. *Materials*, 2021, **14**, P. 1–25.
[2] Wort C.J.H., Balmer R.S. Diamond as an electronic material. *Materials Today*, 2008, **11**, P. 22–28.
[3] Barclay P. E., Fu K.-M., Jelezko F., et al. Diamond photonics: introduction. *J. Opt. Soc. Am. B*, 2016, **33**, P. 1–10.

[4] Dory C., Vercruysse D., Yang K.Y., et al. Inverse-designed diamond photonics. *Nat Commun.*, 2019, **10**, P. 1–7.
[5] Shamrakov A., Efimov P., Alshevsky Yu., et al. Temperature sensors based on a single crys-tal of synthetic diamond. *Nanoindustry*, 2010, **3**, P. 26–28.
[6] Hahl F.A., Lindner L., Vidal X., et al. Magnetic-field-dependent stimulated emission from nitrogen-vacancy centers in diamond. *Sci. Adv.*, 2022, **8**(22), P. 1–9.
[7] Zalieckas J., Greve M.M., Bellucci L., et al. Quantum sensing of microRNAs with nitrogen-vacancy centers in diamond. *Commun Chem.*, 2024, **7**, P. 1–10.
[8] Savvin A., Dormidonov A., Smetanina E., et al. NV – diamond laser. *Nat Commun.*, 2021, **12**, P. 1–8.
[9] Kuriakose A., Chiappini A., Sotillo B., et al. Fabrication of conductive micro electrodes in diamond bulk using pulsed Bessel beams. *Diamond and Related Materials*, 2023, **136**, P. 1–10.
[10] Gramala M., Sikora A., Chudzyńska A., et al. Highly Conductive Paths in Diamond and their Application in High Pressure Measurements. *ACS Applied Materials & Interfaces*, 2024, **16**(43), P. 59528–59535.
[11] Kononenko V.V., Zavedeev E.V., Kononenko T.V., et al. Cleavage-Driven Laser Writing in Monocrystalline Diamond. *Photonics*, 2023, **10**(43), P. 1–10.
[12] Ali B., Xu H., Chetty D., et al. Laser-Induced Graphitization of Diamond Under 30 fs Laser Pulse Irradiation. *J. Phys. Chem. Lett.*, 2022, **13**(12), P. 2679–2685.
[13] Shershnev E.B., Nikityuk Yu.V., Shershnev A.E. Modeling of laser processing of diamond crystals. *Proceedings of Gomel State University named after F. Skorina*, 2011, **6**(69), P. 164–168.
[14] Yuan H., Song C., Zhang C., et al. Simulation study on the effect of different wavelengths of laser on graphitization of diamond surface. *Journal of Physics: Conference Series*, 2023, **2566**, P. 1–7.
[15] Chen Y., Zhang S., Liu J., et al. Numerical Simulation of Temperature Characteristics and Graphitization Mechanism of Diamond in Laser Powder Bed Fusion. *Materials*, 2023, **16**(18), P. 1–7.
[16] Cui X., Li G., et al. Molecular dynamics simulation of laser-induced graphitization of CVD diamond. *Proc. SPIE12169, Eighth Symposium on Novel Photoelectronic Detection Technology and Applications*, 2022, P. 1216941.
[17] Arsentiev M.Y. Investigation of graphitization of diamond surface with orientation [111] using the method of molecular dynamics. *Physics and Chemistry of Glass*, 2021, **47**(3), P. 345–349.
[18] Bukharov D.N., Kononenko T.V., Kucherik A.O. Simulation phenomenological model of laser-induced graphitized structures in diamond. *Letters to the JTP*, 2025, **51**(1), P. 26–29.
[19] Bukharov D.N., Samyshkin V.D., Lelekova A.F., et al. Modeling the structure and electrophysical properties of graphitized regions in artificial diamond. *South Siberian Scientific Bulletin*, 2024, **6**, P. 57–64.
[20] Ferrah I., Benmahamed, Y., et al. A new box-counting-based-image fractal dimension estimation method for discharges recognition on polluted insulator model. *IET Science, Measurements and Technology*, 2025, **19**(1), P. 1-14.
[21] Ashikkalieva K.K., Kononenko T.V., Konov V.I. Graphitization wave in diamond induced by uniformly moving laser focus. *Optics & Laser Technology*, 2018, **107**, P. 204–209.
[22] Kononenko T.V., Komlenok M.S., Pashinin V.P., et al. Femtosecond laser microstructuring in the bulk of diamond. *Diamond and Related Materials*, 2009, **18**, P. 196–199.
[23] Gulina Yu.S. Measurement of the two-photon absorption coefficient of ultrashort laser pulses with a wavelength of 1030 nm on color centers of natural diamond. *Optics and Spectroscopy*, 2022, **130**(4), P. 540–543.
[24] Vaskovskaya M.I., Vasiliev V.V., Zibrov S.A., et al. Amplitude-phase modulation and emission spectrum of a vertical-cavity diode laser. *Quantum Electronics*, 2017, **47**(9), P. 835–841.
[25] Berman R. The diamond-graphite equilibrium calculation: The influence of a recent determina-tion of the Gibbs energy difference. *Solid State Communications*, 1996, **99**(1), P. 35–37.
[26] Kobelev N.P. Khonic V.A. On the Enthalpy and Entropy of Formation of Point Defects in Crystals. *Journal of Experimental and Theoretical Physics*, 2018, **153**(3), P. 409–416.
[27] Shevchenko V.Ya., Perevislov S.N., Nozhkina A.V., et al. High-Temperature Graphitization of Diamond during Heat Treatment in Air and in Vacuum. *Glass Physics and Chemistry*, 2024, **50**(2), P. 115–134.
[28] Roy C.J., Blottner F.G. Review and assessment of turbulence models for hypersonic flows. *Progress in Aerospace Sciences*, 2006, **42**(7–8), P. 469–530.
[29] Benintendi R. *Process Safety Calculations*, Elsevier, Basel, 2018, 300 p.
[30] Ning C.Z., Indik R.A., Moloney J.V. Effective Bloch Equations for Semiconductor Lasers and Amplifiers. *IEEE Journal of quantum electronics*, 1997, **33**(9), P. 1543–1550.
[31] Pimenov V.G. Difference methods for solving partial differential equations with heredity, Yekaterinburg, Ural University Publishing House, 2014, 150 p.
[32] Toumannen B. *GPU programming using Python and CUDA*, Moscow, DMK Press, 2020, 300 p.
[33] Kong Q., Siauw T., Bayen A. *Python Programming and Numerical Methods*, Academic Press, 2020, 210 p.
[34] Grivickas P.P., et al. Carrier recombination and diffusion in high-purity diamond after electron irradiation and annealing. *Appl. Phys. Lett.*, 2020, **117**(24), P. 242103-1–242103-6.
[35] Sze M., Ng K.K. *Physics of Semiconductor Devices*. Hoboken, New Jersey, Simon John Wiley & Sons, Inc., 2006, 832 p.
[36] Wort C.J.H., Balmer R.S. Diamond as an electronic material. *Materials Today*, 2008, **11**(1–2), P. 22–28.
[37] Linnik S.A. Zenkin S.P., Gaidaichuk A.V. Heteroepitaxial growth of diamond from the gas phase: problems and prospects (review). Instruments and experimental techniques, 2021, **2**, P. 5–18.
[38] Stankus S.V., Savchenko I.V., et al. Thermophysical properties of graphite MPG-6. *TVT*, 2013, **51**(2), P. 205–209.
[39] Moelle C., et al. Specific heat of single-, poly- and nanocrystalline diamond. *Diamond and Related Materials*, 1998, **7**(2–5), P. 499–503.
[40] Zhu S., et al. A Revisited Mechanism of the Graphite-to-Diamond Transition at High Temperature. *Matter*, 2020, **3**(3), P. 864–878.
[41] Hannes W.R., Ciappina M.F. Two-photon absorption in semiconductors: A multiband length gauge analysis. *Physical Review B*, 2022, **106**(11), P. 115204.
[42] Smausz T., et al. Determination of UV–visible–NIR absorption coefficient of graphite bulk using direct and indirect methods. *Applied Physics A*, 2017, **123**, P. 633.
[43] Thomas M.E., Tropf W.J. Optical properties of diamond. *Johns Hopkins APL Technical Digest*, 1993, **14**(1), P. 16–23.
[44] Wang X., Chen Y.P., Nolte D.D. Strong anomalous optical dispersion of graphene: complex refractive index measured by Picometrology. *Opt. Express*, 2008, **16**, P. 22105–22112.

[45] Khorkov K.S., Podoprigora Ya.V., Burakova I.V., et al. Synthesis of allotropic forms of carbon in a laser experiment: 1D-3D topological configurations with carbon nanotubes and diamond-like systems. *Bulletin of the Russian Academy of Sciences: Physics*, 2024, **88**(12), P. 2022–2033.
[46] Neff M., Kononenko T.V., Pimenov S.M., et al. Femtosecond laser writing of buried graphitic structures in bulk diamond. *Appl. Phys. A*, 2009, **97**, P. 543–547.
[47] Kononenko V., et al. Highly oriented graphite produced by femtosecond laser on diamond. *Applied Physics Letters*, 2019, **114**, P. 251903.
[48] Bukharov D.N., et al. Mathematical modeling of the structure and optical properties of the fractal island metal nanofilm. *J. Phys.: Conf. Ser.*, 2020, **1439**, P. 012050.
[49] Arakelian S.M., Kucherik A.O., Khudaberganov T.A. et al. Nanophysics in laser-induced cluster systems: topological quantum states in electrical conductivity and features of optical spectra—theory and experiment for dimensional effects. *Opt Quant Electron.*, 2020, **52**, P. 202.

Submitted 12 May 2025; revised 25 July 2025; accepted 26 July 2025

Information about the authors:

Dmitry N. Bukharov – A. G. and N. G. Stoletov Vladimir State University, 87 Gorykogo st, 600000, Vladimir, Russia; ORCID 0000-0002-4536-8576; buaharovdn@gmail.com

Timur A. Khudaiberganov – A. G. and N. G. Stoletov Vladimir State University, 87 Gorykogo st, 600000, Vladimir, Russia; ORCID 0000-0002-2008-7276; thomasheisenberg@mail.ru

Alexey O. Kucherik – A. G. and N. G. Stoletov Vladimir State University, 87 Gorykogo st, 600000, Vladimir, Russia; ORCID 0000-0003-0589-9265; kucherik@vlsu.ru

Sergey M. Arakelian – A. G. and N. G. Stoletov Vladimir State University, 87 Gorykogo st, 600000, Vladimir, Russia; ORCID 0000-0002-6323-7123; arak@vlsu.ru

Conflict of interest: the authors declare no conflict of interest.